Lab on a Chip

Donut-shaped chambers for analysis of biochemical processes at the cellular and subcellular levels.

Journal:	*Lab on a Chip*
Manuscript ID:	LC-ART-12-2013-051426.R1
Article Type:	Paper
Date Submitted by the Author:	03-Apr-2014

Complete List of Authors:	Zurgil, Naomi; The Biophysical Schottenstein Center, Bar Ilan University, Physics Department Ravid, Orit; The Biophysical Schottenstein Center, Bar Ilan University, Physics Department Shafran, Yana; The Biophysical Schottenstein Center, Bar Ilan University, Physics Department Howitz, Steffen; GeSiM - Gesellschaft fuer Silizium-Mikrosysteme mbH, Afrimzon, Elena; The Biophysical Schottenstein Center, Bar Ilan University, Physics Department Sobolev, Maria; The Biophysical Schottenstein Center, Bar Ilan University, Physics Department He, Jian; GeSim - Gesellschaft fuer Silizium-Midrosysteme mbH, Shinar, Eilat; Magen David Adom, Public Cord Blood Bank Lab Goldman-Levi, Ronit; Magen David Adom, Public Cord Blood Bank Lab Deutsch, Mordecai; The Biophysical Schottenstein Center, Bar Ilan University, Israel, Physics Department

Donut-shaped chambers for analysis of biochemical processes at the cellular and subcellular levels.

Zurgil N[1], Ravid O[†1], Shafran Y[†1], Howitz S[†2], Afrimzon E[1], Sobolev M[1], He J[2], Shinar E[3], Goldman-Levi R[3] and Deutsch M[*1]

[1]The Biophysical Interdisciplinary Schottenstein Center for the Research and Technology of the Cellome,Physics Department, Bar Ilan University. 52900, Ramat Gan, Israel.

[2]GeSiMmbH, Bautzner Landstraße 45, 01454 Großerkmannsdorf, Germany.

[3]Magen David Adom Public Cord Blood Bank Lab, Ramat Gan, Israel.

[†]Equal contribution

[*]Corresponding author:

Mordechai Deutsch, Ph.D.

Telephone: 972-3-534-4675

Fax: 972-3-534-1175

E-mail: motti.jsc@gmail.com

Running Headline:

Micro-arrayed donut-shaped chambers for analysis of biochemical processes.

E-mail addresses:

NZ: zurgiln@gmail.com

OR: oritravidh@gmail.com

YS: yana.shafran@gmail.com

SH: howitz@gesim.de

EA: afrimzon@yahoo.com

MS: eweryday@yahoo.com

HJ: jian.he@tu-dresden.de

SE: eilats@mda.org.il

GR: ronitG@mda.org.il

MD*: motti.jsc@gmail.com

Abstract

In order to study cell-cell variation with respect to enzymatic activity, individual live cell analysis should be complemented by measurement of single cell content in a biomimetic environment, on a cellular scale arrangement. This is a challenging endeavor due to the small volume of a single cell, the low number of target molecules and cell motility.

Micro-arrayed donut-shaped chambers (DSCs) of femtoliter, (fL), picoliter (pL), and nanoliter (nL) volumes, have been developed and produced for the analysis of biochemical reaction at the molecular, cellular and multicellular levels, respectively. DSCs are micro-arrayed, miniature vessels, in which each chamber acts as an individual isolated reaction compartment.

Individual live cells can settle in the pL and nL DSCs, share the same space and be monitored under the microscope in a noninvasive, time-resolved manner. Following cell lysis and chamber sealing, invasive kinetic measurement based on cell content is achieved for the same individual cells. The fL chambers are used for the analysis of the same enzyme reaction at the molecular level. The various DSCs were used in this proof-of-principle work, to analyze the reaction of intracellular esterase in both primary and cell line immune cell populations. These unique DSC arrays are easy to manufacture, and offer an inexpensive and simple operating system for biochemical reaction measurement of numerous single cells used in various practical applications.

Key words:

Enzyme

Esterase

Image analysis

In vitro test

Micropatterning

Microstructure

Introduction

Living cells present multiple scales of complexity, ranging from molecules to entire cell populations. Cellular heterogeneity affects the performance of bioprocesses and plays an important role in organism-level outcomes. It has been well demonstrated that cellular variability is closely related to numerous stochastic transcriptional events leading to variations in patterns of expression among single genetically identical cells.[1]

Cells may differ in both their structural and biochemical state, and this variability can be expressed in diverse manifestations. In many cases, cellular heterogeneity becomes evident through the ability of the cell to change its function, shape or chemical composition over time.

Such cellular response is achieved by complex intracellular biochemical reactions and networks that integrate signals transduced from the extracellular environment.

Cell-cell variation in enzyme activity results from interaction between various cell components and multiple cellular processes which occur within the cell volume. As a result, single-cell assays of enzyme activity, particularly those that measure product formation directly, are essential in order to detect and understand intercellular diversity.

In order to understand the biochemical reactions in a single cell system, the dynamic interaction between various biomolecules must be examined under accurate, well-defined, spatial and temporal conditions.

However, in-vitro assays mimicking such environments characterized by ensembles of molecules, each having relatively low number as well as strict spatial constraints, are usually absent.

The most obvious examination of biochemical reaction at the single cell resolution is the single-cell enzyme assays based on optical analysis.[2] In living cells, the behavior of enzymes or other biomolecules can be studied within their physiological context.[3] Practically speaking, living cells are reaction containers at the picoliter level. This feature is important, as biochemical reactions in the cell often occur under non-equilibrium conditions, and interact in complex networks. When measuring live cells using noninvasive optical methods, the spatial and temporal resolution of enzyme activity and its location in subcellular structures becomes available, allowing different states of specific enzymatic activity to be linked to the particular cell function. New advanced techniques and nanotools are being utilized to capture signals from single living cells with high spatiotemporal resolutions for the investigation of cellular processes at the nanoscale level.[4,5] Still, the outcome of such measurement is an overall enzymatic activity in the live cell, and actually comprises many processes and various factors among which are membrane permeability to substrate, substrate efflux (MDR activity), and product retention capabilities.

Thus, the functional analysis of intracellular content as analyzed via image- and flow-based studies of intact cells should be complemented by chemical characterization of cell content (e.g. cell lysates).

In biochemical experiments of cell content, the concentration and the charge state (pH and ionic strength) mimic those of living cells. However, there is also a need to simulate molecular crowding of the cell interior. The interior of the cell is a crowded environment and high concentrations of macromolecules reduce the volume of solvent available for other molecules in the solution, thus increasing their effective concentrations. Due to macromolecular crowding, enzyme assays performed in diluted solutions may fail to reflect the actual process and its

kinetics occurring in the cytosol.[6,7] Consequently, measurements of the properties of enzymes or processes in metabolism that are made in dilute solutions may be different by many orders of magnitude from the true values seen in living cells.[8]

Since the study of biochemical processes under realistically crowded conditions is very important, the analysis of intracellular content of individual cells should be carried out within biomimetic, cellular-scale systems.

Indeed, the small volume of a single cell and the extremely low absolute number of target molecules in cells, render these measurements very challenging.

Many analytical methods, such as optical spectroscopy, electrochemical detection and mass spectrometry, have been successfully used in the context of single-cell analysis.[5,9,10,11,12,13,14,15] Recently, a microfluidic device has been introduced,[16] with enzyme-linked immunosorbent assays (ELISA) for single-cell studies to identify intracellular proteins, secondary messengers, and metabolites. However, very few methods enable correlation between kinetic live-cell measurement and analysis of intracellular content for the same individual cell. In addition, the sophisticated microfluidic devices with a multitude of chambers, valves, and connections are nevertheless impressive, but due to their complexity, are difficult and expensive to produce, and prone to failure. A low cost technique which, on one hand, enables simple manufacturing and operating, and on the other hand, generates a large amount of data from numerous single cells or active molecules, is needed.

In the current study, a novel DSC methodology which addresses the above needs, along with devices to perform biological reactions in fL-nL volume reactors, is presented. DSCs are micro-arrayed, miniature vessels, in which each chamber acts as an individual isolated reaction compartment. Individual live cells can settle in the pL and nL DSCs, share the same space and be

monitored under the microscope in a noninvasive, time-resolved manner. Following cell lysis and segregation of each chamber, invasive kinetic measurement, based on cell content is achieved for the same individual cells. Thus, cell-cell heterogeneity reflected by measurements of both intact cell and cell lysate, become possible.

Materials and methods

Chemicals

RPMI-1640 medium, IMDM medium, heat-inactivated fetal calf serum (FCS), penicillin, streptomycin, glutamine, sodium pyruvate, HEPES and Dulbecco's phosphate-buffered saline (PBS) were obtained from Biological Industries (Kibbutz Beit-Haemek, Israel). Radioimmunoprecipitation (RIPA) lysis buffer (pH 7.4) stock solution contained 10mM Tris-HCl, 1mM EDTA, 0.5mM EGTA, 150mM NaCl, 1% Triton, 0.1% SDS, and 0.1% Na deoxycholate. All chemicals for RIPA lysis buffer, fluorescein diacetate (FDA), dextran, fluorescein, 2 mercaptorthanol and esterase from porcine liver were obtained from Sigma-Aldrich (St. Louis, MO, USA). Ficoll Hypaque PLUS was obtained from GE Healthcare (Piscataway, NJ, USA). NOA81 optical UV adhesive from Norland Products, Inc. (Cranbury, (NJ, USA). SU-8 5 negative tone photoresist was obtained from Microchem Corp. (Newton, MA, USA).

Device Microfabrication

a. The DSC arrays

A 175 μm thick Borosilicate glass (BSG) type D263, was spin coated with negative SU-8 5 photoresist at 3500 rpm using a spin coater RC8 (Suss GmbH, Berlin Germany), resulting in a

photoresist layer of 2-2.5 μm thickness. To ensure good patterning and adhesion of the photoresist layer onto the glass support, immediately after spinning, the coated glass was 'soft baked' (for 1 min at 65°C followed by 3 min at 95°C). Then, the coated glass was UV light illuminated using a patterned Cr-mask which was aligned by mask aligner MA25 (Suss GmbH, Berlin Germany) and thereafter re-soft baked (post UV baking). The illuminated areas of the SU-8 5 photoresist were polymerized by photo-induction to form an array of donuts in accordance with the patterned mask.

Next, the non-illuminated, non-polymerized regions were released from the glass by chemical development, after which the remaining SU-8 5 polymerized regions remained attached to the glass substrate as array of donuts. The formed donut array on glass was then stabilized by thermal annealing at 175°C for 60 min, resulting in a stiff and smooth SU-8 5 donut-structured layer, inseparable from said glass plane support.

Finally, the donut arrayed glass plane was sawed into 5 × 5 mm^2 chips, cleaned (mainly from glass debris) by water jetting, dried with clean compressed air and kept in antistatic bags until fabrication.

b. Slide based DSC array device

DSC arrays were glued onto a standard microscope slide with a small droplet of NOA81 cured by UV light for 25 sec.

Solution loading and array sealing

a. Solution loading procedure

Due to the small dimensions of the DSCs and the hydrophobicity of the SU-8 substrate, liquid is introduced into the chambers by vacuum. Once the chambers are filled with solution, the succeeding steps (e.g cell loading or solution exchange) are facilitated.

To introduce solutions into the DSC, a 40 µl liquid droplet of PBS medium or reaction mixture was poured on top of the DSC array. The liquid was forced into the chambers by vacuum procedure (30-60 sec) using a Low Pressure Plasma Etcher Femto instrument (Diener Electronic GmbH, Ebhausen, Germany).

b. Sealing procedure

The slide based DSC array device is schematically depicted in Figure 1 before and after sealing. Specific actions are taken in order to prevent rapid evaporation of the extremely small volumes of liquid within the DSCs. An additional aliquot of solution (200 µl) is poured on top of the pre-loaded array to prevent solution drying during sealing procedure. The liquid is covered with a layer of 0.010" thick silicon sheet (silicon sheeting NRV G/G 40D 12" × 12" from Specialty Manufacturing Inc., (Saginaw, MI, USA) and pressed (Figure 1a). Upon pressure, the solution between the individual DSCs is thrust aside, while the content of the chambers remains unaffected (Figure 1b). The overflow liquid is surrounded by a strip of grease, Silicon-Hochvakuumfett schwer (Merck, Darmstadt, Germany) in order to avoid dehydration. A microscope slide was placed on top of the silicon sheet. The upper and lower microscope slides were pressed hard with clamps in order to seal the DSC array and prevent liquid evaporation. The DSC array device was mounted on the microscope stage for measurement.

Image acquisition and analysis

a. Imaging system and operating software

Images were acquired using a motorized Olympus inverted IX81 microscope (Olympus Corporation, Tokyo, Japan). The microscope is equipped with a sub-micron Marzhauser-Wetzlar motorized stage type SCAN-IM, with an Lstep controller; (Marzhauser Wetzlar GmbH, Wetzlar, Germany) and a filter wheel including fluorescence cube (excitation filters, dichroic

mirrors, and emission filters, respectively) for fluorescein: 470-490 nm, 505 nm long pass and 510-530 nm, for DSC auto-fluorescence: 355-405 nm, 410 nm long pass and 420-450 nm. All filters were obtained from Chroma Technology Corporation (Brattleboro, VT, USA). Objectives of ×4/×10, ×20 and ×60 were used for the nL, pL and fL DSCs, respectively. A cooled, highly sensitive 14-bit, ORCA II C4742-98 camera (Hamamatsu Photoics, Hamamatsu, Japan) was used for imaging. Olympus Cell^P software was used for image analysis (Olympus Corporation, Tokyo, Japan).

b. Image analysis

For optical data acquisition and analysis, each set of image acquisitions was initiated by first acquiring the bright-field image of a chosen view field, followed by the acquisition of two fluorescence images; one for fluorescein and the other for the structure auto-fluorescence, each taken at a different preset time point. Data was then filtered to disregard chambers with more than a single cell. DSCs were defined as Objects of Interest and outlined on the bright field image. Then, on each fluorescent wide field image, objects of interest were determined by mapping those outlines on the interrogated fluorescent field image. Next, the fluorescent background, determined by averaging the fluorescence intensity (FI) detected by camera pixels found between the outlined regions, was subtracted from the fluorescent image. It should be emphasized that background signal determination and subtraction were performed separately for each of the acquired fluorescent field images. The mean FI value obtained from each DSC (all pixels within DSC area) was normalized to the mean background intensity value obtained from empty chambers in the same region.

For FI(t) measurement, following background measurement, DSC arrays were exposed to FDA substrate, sealed and sequentially imaged 6-8 times at intervals of 5-10 min. This yielded 6-8

accurately timed FI data points per chamber, from which the reaction rate (slopes) was extracted as described below in *Characterization of cellular enzymatic activity.*

Cell volume evaluation

Since the Molt-4 T cells and umbilical cord blood (UCB) cells used in this study are spherical in shape, cell diameter was extracted by two procedures:

(a) directly measuring the radius (r) on the largest 2D image projection (S) by crossing S with a few profile lines and counting the number of pixels along them, from which the cell volume $V_c = \frac{4\pi}{3} r^3$ was calculated.

(b) defining the cell as a Region of Interest (ROI), from which, utilizing the Olympus Cell^P software, the area S_{ROI} of said ROI was defined, and cell volume was calculated using the formula

$$V_c = \frac{4\pi}{3} r^3 = \frac{4\pi}{3} \left(\frac{S_{ROI}}{\pi}\right)^{\frac{3}{2}} = (4/3) {S_{ROI}}^{3/2} \pi^{-1/2}$$

Both procedures yielded similar results (see Supplementary Information). The mean cell volume of the T cell line was 2753 ± 494.50 fL, while the averaged cell volume of the primary UCB cells was 380.5 ± 335.8 fL.

The effects of volume estimation error on the measurements of enzyme reaction rates within DSCs are thoroughly discussed in Supplementary Information.

Chamber dimensions evaluation

Evaluation of chamber dimensions was accomplished by extracting chamber diameter from SEM (pL DSC) and AFM (fL DSC) images, as well as from the bright field and UV auto-fluorescence images of the array structures. Chamber depth was evaluated from SEM (pL and nL DSC) and

from AFM (fL DSC) images. Good correlation was found between the calculated dimensions from all types of images that were used (See Supplementary Information).

Evaluation and correction of photobleaching

In control experiments, the photobleaching rate of the fluorescent product was determined by enclosing Fluorescein standard solutions at various concentrations in the DSCs, and monitoring the fluorescence decrease by acquiring sequential images under the same exposure and preset time conditions as the enzymatic reaction experiments.

The raw FI values of each chamber were corrected by employing the calibration factor from the appropriate corresponding control photobleaching curve.

Evaluation of DSC sealing and chamber crosstalk

For the estimation of chamber crosstalk, pre-stained cells were used as a tool to enclose fluorescent solution within a few distinctive DSCs in the array. Upon cell lysis, only those chambers occupied by cells showed fluorescent signals, which when monitored, revealed chamber crosstalk. Molt-4 T cells were stained in-tube by FDA (2.4 μM 10 min) at RT, washed twice with fresh PBS and loaded at low concentration on pL DSC array. After acquisition of bright field and fluorescence images, in-DSC cell lysis was initiated, the array was sealed and imaged after 100 min.

Characterization of cellular enzymatic activity

a. Human T cell leukemia cell line

Molt-4 cells were maintained in RPMI-1640 medium, supplemented with 10% heat-inactivated fetal calf serum (FCS), 100 U/mL penicillin, 100 μg/mL streptomycin, 2% glutamine, 2% sodium pyruvate and 2% HEPES.

b. Umbilical cord blood (UCB) cells

UCB units from healthy newborns were obtained from Magen David Adom Public Cord Blood Bank (MDA, Tel Hashomer, Israel). The study with UCB cells was certified at the Magen David Adom Public Blood Bank and conducted under regulations in accordance with the Helsinki Declaration. Red blood cells were sedimented using dextran, and thereafter mononuclear cells were isolated using Ficoll-Hypaque. UCB cells were maintained in IMDM medium supplemented with 1% penicillin and streptomycin, 30% FCS and 7.5×10^{-5} M 2-mercaptoethanol in completely humidified atmosphere with 5% CO_2 at 37°C. Before use, cells were collected, washed and suspended in PBS at appropriate concentrations.

c. Cell loading

In order to load cells into the array, DSCs must first be wetted and filled with buffer by vacuum procedure as described. Then a cell suspension (10 µl, 5×10^6 cells/ml in PBS) is loaded on top of the DSC array, and cells allowed to settle by gravity for 5-10 min. Excess cells are gently washed away with PBS (aliquots of 10-20 µl) under microscope observation. During live cell measurements, the DSC array is open, and individual cells settle in the unsealed chambers, sharing common space and medium. For cell content analysis, at the conclusion of live cell measurements, the volume on top of the array is reduced to less than 4 µl, and a 200 µl aliquot of lysis buffer mixed with FDA is dispensed on top of the array, and immediately the sealing procedure is carried out as described above in *Solution loading and array sealing*.

d. Preparation and analysis of bulk cell lysate

For preparation of whole-cell lysates from bulk cell populations (bulk cell lysate), suspensions of live Molt-4 T cells were transferred to a 15 ml tube and washed twice by centrifugation at 3000 rpm for 5 min. The pellet was suspended in RIPA lysis buffer (1:20) at cell concentration

of 7×10^4 cells/ml, vortexed, and the tube was allowed to stand for 20 min at RT. Cell debris was not removed. Control measurements of esterase activity in bulk cell lysate were carried out in a microtiter plate, by mixing the lysate 1:1 with FDA solutions (final concentrations of 5-50 μM) and detecting the changes in FI of the product during time via both the imaging system and by VICTOR3™ V 1420 Multilabel Plate Reader (PerkinElmer, Waltham, MA, USA). Good correlation was found between both measurement systems (data not shown).

For in-DSC esterase reaction measurements, bulk cell lysate was mixed in a tube 1:1 with FDA solution (96 μM), and immediately loaded onto the DSC (nL and fL), sealed as described above and imaged over the course of about 1 h at intervals of 5-10 min. The time delay between lysate mixing with FDA and the start of the imaging procedure was about 5 min.

Reaction rate was determined by calculating the average slope of the curve. This was done by averaging the 6-8 slopes of the lines drawn between each two data points on the graph of FI(t). In many cases, under the conditions used here, the average slope was not significantly different from the slope of the best-fit straight line that was drawn using linear regression function.

e. Preparation and analysis of single cell lysate

Ten μl of cell suspension aliquot (5×10^6 cells/ml in PBS) were applied on top of the wetted pre-filled chambers , and cells allowed to settle by gravity for 5-10 min. Excess cells were gently washed away by PBS (aliquots of 10-20 μl) under microscope observation, and reference bright field images were acquired. For in-DSC cell lysis, the volume of the solution above the cells within the array was reduced (< 4 μl) and a mixture (200 μl) of RIPA (final dilution 1:20) and FDA (final concentration 48 μM) was added on top of the trapped cells, and immediately the sealing procedure was performed (as described above). The dilution of FDA concentration due to

the residual PBS within the chambers did not exceed 2%. The time delay between the addition of FDA in lysis buffer and the start of image acquisition was about 4 min. The array was sequentially imaged over the course of 1 h at intervals of 10 min, yielding 6-8 accurately timed FI data points per each individual cell/chamber. For both cell types, the individual cell FI(t) was found to be linear within the time frame of the experiment. The enzymatic reaction rate for each individual cell was calculated from the slope of the best-fit straight line that passed between time points 10 min and 60 min.

f. Monitoring intracellular esterase reaction in live cells

FDA hydrolysis by non-specific esterase was measured in live Molt-4 and UCB cells as described.[17] Cells were loaded within pL DSCs and washed with PBS. Cells within the open (non-sealed) DSC array were exposed to FDA (1.2 μM in PBS) and time-dependent FI signals were acquired (8 images at intervals of about 90 sec). The enzymatic reaction rate of each individual cell was calculated from the slope of the straight line passing through the 8 time points.

g. Purified enzyme reaction

Esterase from porcine liver (Sigma, cat no: E3019) was dissolved in reaction buffer: 20 mM Tris (pH = 8), 150 mM NaCl, 0.01% Triton X-100. FDA substrate was added to the enzyme solution for the onset of the reaction and the solution was immediately loaded onto the fL DSC array and sealed as described. Images were acquired at specific time points for kinetic measurement of product formation. Reaction rates were calculated from the slopes of the straight lines that were best fitted by linear regression function.

Scanning Electron Microscopy (SEM)

The DSC arrays were coated with gold (up to 10 nm), and studied using a scanning electron microscope (Inspect, FEI, Hillsboro, OR, USA).

Atomic Force Microscopy (AFM)

Atomic force microscopy measurements were carried out with the NanoScope Dimension 3100 controller (Digital Instruments, Inc. NY, USA).

Statistical analysis

For each experiment, two to three DSC arrays were used (500, 200 and 100 chambers for the fL, pL, and nL arrays respectively). For each device, a total of four images were acquired (one each from four different representative areas). Mean and SD for the measured parameter were calculated for each array, and data presented as mean Fluorescence Intensity (FI) ± SD of all pixels within area of each chamber, or averaged FI ± SD for all chambers in an array.

Comparison between cell groups or reaction chambers was carried out using a Student's t-Test with statistical significance set at $p < 0.05$. Single factor ANOVA test was used for estimating the stability of FI variances.

Results

Device microfabrication

Homogeneous arrays of three types of DSCs were fabricated directly on surfaces using SU-8, an epoxy-based photoresist, and high aspect ratio structures were made.

SU-8 was found to be compatible with cell culturing and protein analysis (data not shown). The polymer microstructure arrays (SU-8) are optically transparent in the visible spectrum, enabling a clear visualization of individual cells or cell groups in visible light.

Scanning electron microscopy, AFM and bright field images showed regularly spaced, uniform donut-shaped chambers for all types of chamber arrays (Figure 2).

Auto-fluorescence of the polymers at the UV range was used to visualize the geometry of the micro-structures via UV fluorescence emission light and to estimate structure size and uniformity (Figure 3). Dimensions and volumes of the three types of DSCs are summarized in Table 1.

Uniformity of the embossed chamber arrays was high, with small variations between different DSCs. The mean diameter of the nL, pL and fL DSCs (as measured from SEM, AFM, transparent light and UV fluorescent images) was 241 ± 2.8 μm (n = 18), 25.6 ± 0.67 μm (n=600) and 2.57 ± 0.19 μm (n = 130), correspondingly.

The average height (as measured via SEM and AFM) was 90.4 ± 8.09 μm, 25.01 ± 2.89 μm and 1.97 ± 0.21 μm for the nL, pL and fL DSCs, respectively.

Typical coefficient of variation (CV) of the wall height was 2.5% and that of the chamber diameter was about 10%.

System validation and control measurements

a. Uniformity of the fluorescence signals

For estimation of the variations in the fluorescence signals, each type of DSC array was filled with fluorescent solution. Images were acquired and the FI of individual chambers (mean FI of all pixels within area of each chamber) was analyzed. Figure 3 depicts the **n**L, pL and fL DSC arrays filled with fluorescein solution.

Following sealing of DSCs, the FI signals measured in individual chambers were homogeneously distributed throughout the array. The averaged CV of fluorescein solution signals was 9.4% for the pL DSC, 7.45% for the nL DSC and 14.1% for the fL DSC.

b. Calibration of fluorescein concentration

For calibration of product fluorescence signals, each type of DSC array was filled with a series of fluorescent solutions at various fluorescein concentrations. Images were acquired and the

intensity of the measured fluorescence (average of four images per solution) was plotted as a function of fluorescein concentration. Increasing fluorescein concentration resulted in a dose-dependent increase of the intensity emitted (Figure 4). Under the same image acquisition conditions, calibration curves obtained for fluorescein levels measured in all three types of DSCs showed good linearity within the range of fluorescein concentrations used. All three plots were best fitted with linear regression functions (R^2 = 0.996, 0.999, 0.997 for the fL, pL and nL DSCs, respectively).

The detection limit for each type of DSC was determined to be the lowest fluorescein concentration that was statistically different from the blank (e.g. DSC filled with PBS).

Under the conditions used here, the detection limits of fluorescence based measurements within the DSCs were 5 μM, 1 μM and 0.1 μM for the fL, pL and nL DSCs, respectively (Table 1). The higher sensitivity of the larger chambers can be explained by the high positive correlation of FI signals with the height of the DSC. The number of fluorescein molecules at the particular detection limit concentrations in a given corresponding chamber volume was calculated.

It was found that the minimum expected number of fluorescein molecules that can be detected was as little as 1×10^4 for the fL DSC, 7.3×10^6 for the pL DSC, and 3×10^8 molecules for the nL DSC (Table 1). Since a typical mammalian cell with a 10 μm diameter and a volume of 500 pL contains about 1×10^9 total protein molecules derived from about 1×10^4 different protein types,[18] the estimation of 1×10^5-10^7 molecules per specific protein is realistic for the detection of a single type of molecule within pL DSC, among the ensemble of biomolecules derived from a single cell. Obviously, an increase of sensitivity by signal intensification may be

generated either by amplifying the molecule of interest or by attaching labels that intensify the signal.

c. Evaluation of DSC sealing and chamber crosstalk

For the estimation chamber leakage, pre-stained cells were used as a tool to enclose fluorescent solution within a few specific DSCs. Following cell lysis and array sealing, only chambers which were occupied by cells showed fluorescent signals, which, when monitored, revealed chamber crosstalk. Figure 5 depicts six representative individual pL DSCs 100 min following cell lysis and chamber sealing. As can be seen, although high FI is detected in the three chambers occupied by cells, the area in-between chambers, as well as the adjacent empty chambers showed negligible fluorescence. The averaged FI of all occupied DSCs was 550.8 ± 411, while that of empty chambers and in-between regions was significantly lower 0.54 ± 4.9 ($p < 0.005$, $n = 100$), indicating that no crosstalk or chamber leakage was observed throughout the experiment. The high variation in the mean FI of these DSCs stems from the inherent initial FI variation between individual stained cells, as measured on the array before cell lysis (CV for population average FI 38.1%). In a complementary experiment, where unlabeled cells were loaded in pL chambers, and lysis and FDA staining occurred in-DSC, similar results were achieved (data not shown).

Characterization of cellular enzymatic activity within DSC

To establish the feasibility for in-DSC cell lysis and the detection of enzyme reactions, the activity of nonspecific esterase was evaluated at the multicellular, cellular and molecular levels. Bulk cell lysate, as well as individual cell lysate were measured via the pL and nL vessels, while the activity of pure enzyme preparation was analyzed using fL DSC.

For the analysis of esterase activity, the fluorogenic substrate (FDA) was simply mixed either with the pure enzyme or with cell lysate preparation, enclosed in the chambers, and the array was

sequentially measured. As the substrate concentration is much higher than that of the enzyme, and since each chamber holds the same amount of substrate, the reaction rate is proportional to the number of enzyme molecules in each chamber.

a. Analysis of bulk cell lysate

Bulk cell lysate derived from Molt-4 T cells was mixed with FDA (final concentration 48 μM), immediately loaded on the nL and pL DSCs, sealed and measured over the course of 1 h. The hydrolysis of FDA within the two types of DSCs is plotted in Figure 6. As can be seen, in both chambers, esterase activity is evident under the conditions used here. The average rate of product formation was 70.4 ± 8.2 nM and 68.2 ± 5.5 nM fluorescein per min for the pL and nL DSCs, respectively, ($p = 0.2$) indicating the comparable rate of fluorescein production in the two types of chambers.

Considering the original number of cells (3.45×10^6 cell /ml) from which the lysate was prepared, and the DSC volumes, it has been observed that the reaction rates within a single nL DSC (volume of 4.9 nL) was obtained from active molecules derived from 14 cells, while the activity in a single pL chamber was derived from only 0.035 cell (volume of 12.2 pL). Hence, it is reasonable to assume that under the conditions used here, esterase reaction will be detected within the content of a single cell.

b. Analysis of esterase activity in single cell lysate

For esterase activity measurement in single cell lysate, live cells were first loaded into pL DSCs, lysis buffer mixed with FDA was added and the chambers were immediately sealed and measured.

Kinetic measurements of esterase activity in individual Molt-4 and individual primary UCB cell lysate are shown in Figures 7 and 8 respectively. The cells were first loaded into the pL

chambers and bright field images were acquired (Figure 7a, Figure 8a). Investigating cell morphology before their destruction shows that individual primary UCB cells are much smaller than Molt-4 T cells. Following washing of the excess cells, individual chambers that hold single cells are evident (Figure 7b, Figure 8b), as the chambers become fluorescent upon cell lysis, reaction initiation and chamber sealing (Figure 7c, Figure 8c). Since cell content was diluted to a finite volume of an fL DSC (12265 fL), for each cell/chamber the FI was corrected by the appropriate dilution factor.

Kinetic measurement of representative individual Molt-4 T cell lysates is illustrated in Figure 7d. Fluorescence trajectories of 20 corresponding pL DSCs are shown. The slope of these trajectories is used to calculate the enzymatic reaction rates for every single cell lysate. Measurements of the same enzyme reaction in UCB individual cell lysate are illustrated in Figure 8d.

High heterogeneity is manifested within reaction rates of Molt-4 T cell lysate as well as those of cord blood cells. Density histograms of the observed reaction rates derived from individual Molt-4 and UCB cells are shown in Figure 9a. The dispersion of enzyme activity within T cell content and in the blood cell lysates was high; with a coefficient of variation (CV) 75% and 89% for the Molt-4 cell lysate and UCB cell lysate, respectively. The averaged slope for the Molt-4 T cell lysate (40.75 ± 30.6 au) was significantly higher than the averaged reaction rate of UCB cell lysate (17.77 ± 15.7 au, $p < 0.001$).

c. Intracellular esterase reaction in live cells

FDA is a non-fluorescent molecule which easily penetrates the live cell membrane. Upon cell entrance, the ester bonds of FDA are hydrolyzed by intracellular esterases, generating fluorescein molecules which accumulate within the cell.

When intracellular esterase activity is measured in individual intact cells captured within pL DSCs, the two cell types display significant differences in their slopes (Figure 9b), indicating a marked distinction in their velocity for hydrolyzing FDA. The averaged reaction rate of the T cell line was 156. 4 ± 40.07 au, while that of the primary blood cells was 13.3 ± 6.38 au. Distribution of slopes in the intact live cell populations was lower than their corresponding lysates (CV values of 25% and 48% for the Molt-4 T cells and UCB cells, respectively).

The low reaction rates that were found in intact UCB cells may be attributed either to the enzymes (small number of enzyme molecules, or their low activity) or to the cell membrane properties (high MDR activity,[19] low retention of product). It should be noted that within both cell groups, no positive correlation was found between cell volume and enzyme reaction rate. (Pearson correlation – 0.063 and 0.032 for the Molt-4 T cells and UCB cells, respectively).

As shown above via analysis of individual cell lysate, the net enzyme activity in primary cell lysate is lower than that of Molt-4 cells even after correction for the dilution of each cell's content within the pL DSC.

Taken together, it can be concluded that differences between Molt-4 T cells and UCB cells originate not only from size differences (which may reflect the number of enzyme molecules per cell) or membrane properties, but from additional inherent factors, including actual activity of the enzyme, which influence both intra-population and inter-cell group heterogeneity in enzyme activity.

d. Esterase reaction in cell-groups via nL DSC

When cell suspension was introduced into the nL DSC, groups of various cell numbers settled inside the chamber (Figure 10a,c). Following cell lysis, (Figure 10b) overall enzymatic activity

of all the cells trapped in a single chamber is exposed (Figure 10d) and expressed by the increase in FI profile of horizontal line across the chamber walls (Figure 10e).

The DSC methodology enables correlation between cell number and total rate of reaction. Indeed, a positive correlation was found between the number of cells trapped within an nL chamber and reaction rate (slope). However, analyzing the slopes derived from the same amount of cells showed about 30% variation, indicating that population heterogeneity within these small cell groups, and the specific cell content of each DSC determined the final rate of enzymatic reaction (Figure 10f).

e. Measuring purified enzyme reaction in fL DSC

The fL DSC was used for the analysis of purified esterase enzyme. The reaction rates of esterase from porcine liver were measured at three different enzyme concentrations. (See Figure S2). Under the conditions used here, the rate of reaction increased linearly with the increase in enzyme concentration (R^2 = 0.998). The mean rate of product formation (fluorescein) was 0.34 μM fluorescein per min per 1 enzyme unit. Calculating the rate of fluorescein formation by a single cell lysate, (0.03 μM per min), and comparing it to that of the purified enzyme, one can assume that the averaged enzyme concentration in a single Molt-4 T cell is equivalent to 0.1 unit of purified enzyme.

Discussion

Phenotypically uniform cell populations may contain subpopulations with different activities of enzymes, membrane transporters, and other functional units. Specific technology and devices are required for the detection and characterization of such inter-cellular heterogeneity. The current study offers innovative analytical tools for the detection and characterization of biological

molecules and processes that occur within individual cells in populations. This has been realized by designing and producing a single-cell donut-shaped, pL volume chamber, which can temporally and spatially control the chemical and biological environment.

The pL DSC enables live cell measurement while the chambers share the same media. Once the cells are enclosed within the DSC, they are confined in the vessel and can be lysed. Validation studies demonstrated here that following cell lysis and DSC sealing, analysis of the content of each cell in a cellular-scale arrangement is facilitated.

The basic principle of the pL DSC further evolved into both a larger, nL scale DSC, to enable analysis of small cell groups or cell clusters, as well as into a smaller, fL DSC, which is an ultra-sensitive biochemical-molecular tool, down to single molecule detection.

In most devices which are used for single cell analysis, cells are captured in miniature cavities or holes with finite volume.[20,21,22] In contrast to these widely used holes/wells, the DSC walls are higher than the interspace between them. This unique feature facilitates retention of fluid content in each chamber when the liquid between the chambers is removed, and thus prevents crosstalk or leakage between adjacent chambers following sealing. This quality was demonstrated by loading and lysing pre-stained cells within pL DSCs. Following cell lysis and array sealing, initial heterogeneity in individual live cell fluorescence signals was preserved, while no leakage from the chambers was evident.

Several analytical tools for characterizing single cell content have been presented using various methods.[18,23] However, only few studies offer the combination of live-cell functional measurement and analysis of cell content for the same individual cells.

The combination of live-cell functional measurement and cell substance analysis has been allowed only in cases where one of the analytes was restricted to a solid phase. For example, the

detection of gene expression and secretion of antibodies in single cells as demonstrated by Gong et al[24] was allowed by immobilizing the antibodies, or the sequential measurements of nitric oxide generation rates and the levels of its synthase enzymes, in which the latter were quantified by immunohistochemistry.[25] The current technology uniquely facilitates the correlation between enzymatic parameters of a single cell measured in solution, and its other functional or structural properties.

Chemical analyses of single cell constituents frequently involve complex procedures for cell separation, lysis and extraction of intracellular components.[9,26] Most of these techniques use capillaries and sophisticated micro-fabricated fluidic devices which cannot handle parallelized treatment of numerous cells.[27] The DSC methodology is well suited for simultaneous and uncomplicated on-chip separation and lysis of large populations of single cells, and can potentially be used in high-throughput fashion.

The standard lysis buffer applied here provides a lysis time of seconds, which is relatively slow compared to optical or electrical lysis,[28] but appropriate for esterase reaction analysis since cell destruction is faster than cellular process kinetics (e.g. enzyme reaction) that was investigated. This chemical lysis is not technically complex, and has a low degree of cell type and analyte specificity. Using the current prototype device, a delay time of several minutes occurred between reaction onset and the first measurement, which was mainly attributed to the array sealing procedure and alignment of the device on the microscope stage, a technical issue which can be improved on, in the future.

Functional demonstration of enzymatic activity in live individual cells, as well as in their lysate, was accomplished by monitoring the activity of non-specific esterase. Esterases are responsible for hydrolytic biotransformation of endogenous substrates and are critical for various

biological processes. Located in the endoplasmic reticulum and cytosol, esterases are widely distributed among tissue, and play a major role in drug metabolism and pro-drug activation.[29,30] Using our line of DSCs, intercellular heterogeneity in esterase activity has been exposed. Such information is pharmacologically and toxicologically important, since these serine enzymes serve as biosensors for detection of organophosphorus compounds and other cholinesterase inhibitors.

The current proof-of-principle work utilizes two immune cell populations – T cell line and primary UCB cells. Variation in enzyme concentration and enzyme activity between cell types, as well as between individual cells within populations, were demonstrated by analyzing individual cells or small cell groups. The Molt-4 cells showed significantly higher FDA hydrolysis rates, both in intact cells and in cell lysate, indicating an intrinsic higher concentration or activity of intracellular esterases in these cells.

Immune cell populations which feature a high level of phenotypic variability, are heterogeneous in their gene expression patterns, and show various responses to specific antigens as part of their function. Therefore, these cell populations are especially compatible for measurements on a single-cell level.[31] Such studies are challenging due to the non-adherent nature of the cells, which prevent the spatial preservation of cells during experiments. Hence, most research at the level of single immune cells uses non-invasive imaging methods in combination with microfluidic technologies[32] or with micro-wells,[22,31] and is based mainly on the monitoring of cellular processes via the fusion of fluorophore moiety to proteins or enzymes of interest. As shown here, DSC technology facilitates the use of non-transfected primary immune cells, not only for the live functional imaging, but also for the enzymatic reaction in solution.

A concept for analysis of a single cell at the single-molecule level on a microchip has recently been suggested by Xu et al.[33] This concept may easily be achieved using DSC technology, by integrating both the pL and fL chambers on the same array, enabling cell based and cell free (molecular) assays on a single device.

Conclusions

The microarrayed miniature vessels in a range of volumes (fL to nL) are easy to manufacture, and offer an inexpensive and simple system for various biochemical reaction measurements, both for practical applications and fundamental research.

In addition to live cell analysis and the corresponding single cell content, the arrayed DSCs can be integrated into high throughput biochemical reaction systems, yielding high-density, low-volume assays for analysis of small chemical compounds, peptides, and proteins, in drug discovery and biological synthesis.

Acknowledgements

This study was endowed by the Bequest of Moshe-Shimon and Judith Weisbrodt.

References

1. F. Mannello, D. Ligi, and M. Magnani, *Expert Review of Proteomics*, 2012, **9(6)**, 635-648.
2. M. L. Kovarik and N. L. Allbritton, *Biotechnol,* 2011, **29(5)**, 222-230.
3. D. G. Spiller, C. D. Wood, D. A. Rand and M. R. H. White, *Nature*, 2010, **465(7299)**, 736-745.
4. X. T. Zheng and C. M. Li, *Chem Soc Rev* 2012, **41(6)**, 2061-2071.
5. M. L. Kovarik, P. C. Gach, D. M. Ornoff, Y. Wang, J. Balowski , L. Farrag and N. L. Allbritton, *Anal Che*m, 2012, **84(2)**, 516-540.
6. E. D. Levy, S. De and S. A. Teichmann, *Proc. Natl. Acad. Sci. U.S.A.,* 2012, **109(50)**, 20461-20466.
7. M. G. S. Norris and N. Malys, *Biochem Biophys Res Commun,* 2011, **405(3)**, 388-392.
8. A. P. Minton, *J Cell Sci,* 2006, **119(Pt 14)**, 2863-2869.
9. F. S. O. Fritzsch, C. Dusny, O. Frick and A. Schmid, *Annu Rev Chem Biomol Eng,* 2012, **3**, 129-155.
10. M. He, J. S. Edgar, G. D. M. Jeffries, R. M. Lorenz, J. P. Shelby and D. T. Chiu, *Anal Chem,* **2005, 77(6)**, 1539-1544.
11. L-F. Cai, Y. Zhu, G-S. Du and Q. Fang, *Anal Chem,* 2012, **84(1)**, 446-452.
12. P. N. Nge, C. I. Rogers and A. T. Woolley, *Chem Rev,* 2013, **113(4)**, 2550-2583.
13. H. Yin and D. Marshall, *Current Opinion in Biotechnology,* 2012, **23(1)**, 110-119.
14. Y. Sasuga, T. Iwasawa, K. Terada, Y. Oe, H. Sorimachi, O. Ohara and Y Harada, *Anal Chem,* 2008, **80(23)**, 9141-9149.
15. D. Irimia, R. G. Tompkins and M. Toner, *Anal Chem,* 2004, **76(20)**, 6137-6143.

16. K. Eyer, S. Stratz, P. Kuhn, S. K. Küster and P.S. Dittrich, *Anal Chem,* 2013, **85(6)**, 3280-3287.

17. N. Zurgil, E. Afrimzon, A. Deutsch, Y. Namer, Y. Shafran, M. Sobolev, Y. Tauber, O. Ravid-Hermesh and M. Deutsch, Polymer live-cell array for real-time kinetic imaging of immune cells. *Biomaterials*, 2010, **31(18)**, 5022-5029.

18. A. Schmid, H. Kortmann, P. S. Dittrich and L. M. Blank, *Current Opinion in Biotechnology,* 2010, **21(1)**, 12-20.

19. V. Koshkin and S. N. Krylov, *Anal Chem,* 2013, **85(5)**, 2578-2581.

20. Y. Men, Y. Fu, Z. Chen, P. A. Sims, W. J. Greenleaf and Y. Huang, *Anal Chem,* 2012, **84(10)**, 4262-4266.

21. H. H. Gorris and D. R. Walt, *Angew Chem Int Ed Engl,* 2010, **49(23)**, 3880-3895.

22. M. Polonsky, I. Zaretsky and N. Friedman, *Brief Funct Genomics,* 2013, **12(2)**, 99-108.

23. N. J. Dovichi and S. Hu, *Current Opinion in Chemical Biology,* 2003, **7(5)**, 603-608.

24. Y. Gong, A. O. Ogunniyi and J. C. Love, *Lab Chip,* 2010, **10(18)**, 2334-2337.

25. Y. Shafran, N. Zurgil, E. Afrimzon, Y. Tauber, M. Sobolev, A. Shainberg and M. Deutsch, *Anal Chem*, 2012, **84(17)**, 7315-7322.

26. R. N. Zare and S. Kim, Microfluidic platforms for single-cell analysis. *Annu Rev Biomed Eng*, 2010, **12**, 187-201.

27. J. S. Mellors, K. Jorabchi, L. M. Smith and J. M. Ramsey, Integrated microfluidic device for automated single cell analysis using electrophoretic separation and electrospray ionization mass spectrometry. *Anal Chem*, 2010, **82(3)**, 967-973.

28. K. S. Phillips, H. H. Lai, E. Johnson, C. E. Sims and N. L. Allbritton, Continuous analysis of dye-loaded, single cells on a microfluidic chi. *Lab Chip*, 2011, **11(7)**, 1333-1341.

29. J. J. Prusakiewicz, C. Ackermann and R. Voorman, *Pharm Res,* 2006, **23(7)**, 1517-1524.

30. P. Masson, E. Carletti and F. Nachon, *Protein Pept Lett*, 2009, **16(10)**, 1215-1224.

31. K. Guldevall, B. Vanherberghen, T. Frisk, J. Hurtig, A. E. Christakou, O. Manneberg, S. Lindstr□m, H. Andersson-Svahn, M. Wiklund and B. □nfelt, *PLoS ONE,* 2010, **5(11)**, e15453.

32. D. Di Carlo, N. Aghdam and L. P. Lee, *Anal Chem,* 2006, **78(14)**, 4925-4930.

33. Y. Xu, K. Jang, T. Yamashita, Y. Tanaka, K. Mawatari and T. Kitamori, *Anal Bioanal Chem,* 2012, **402(1)**, 99-107.

Figures

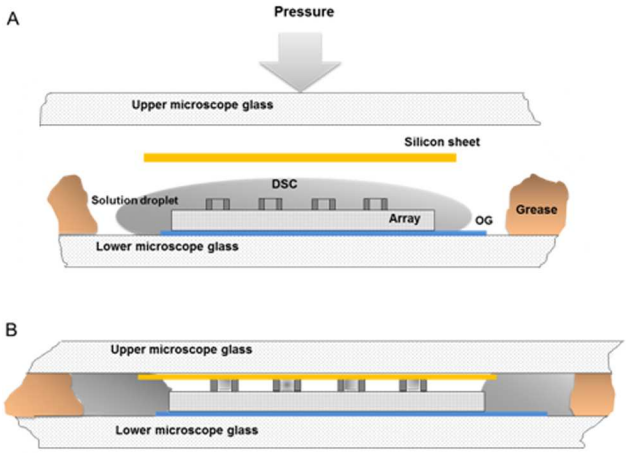

Figure 1

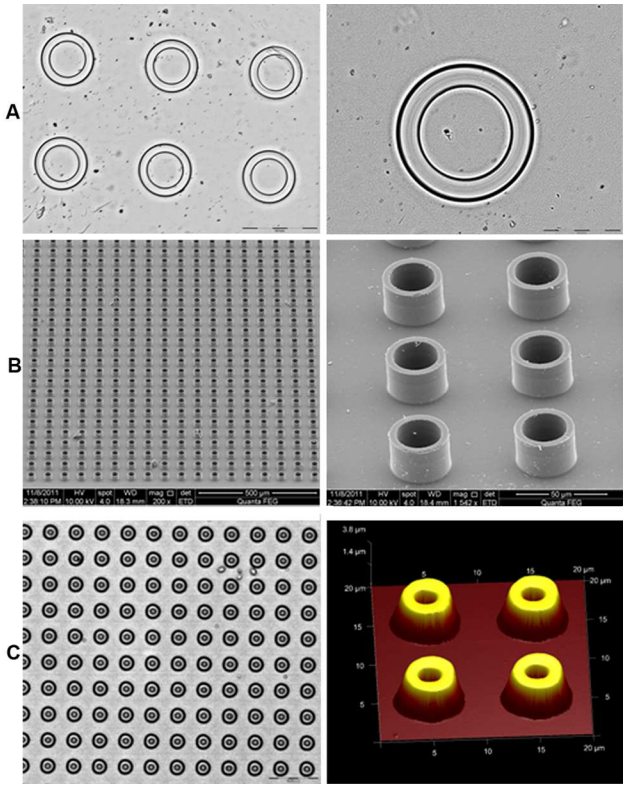

Figure 2

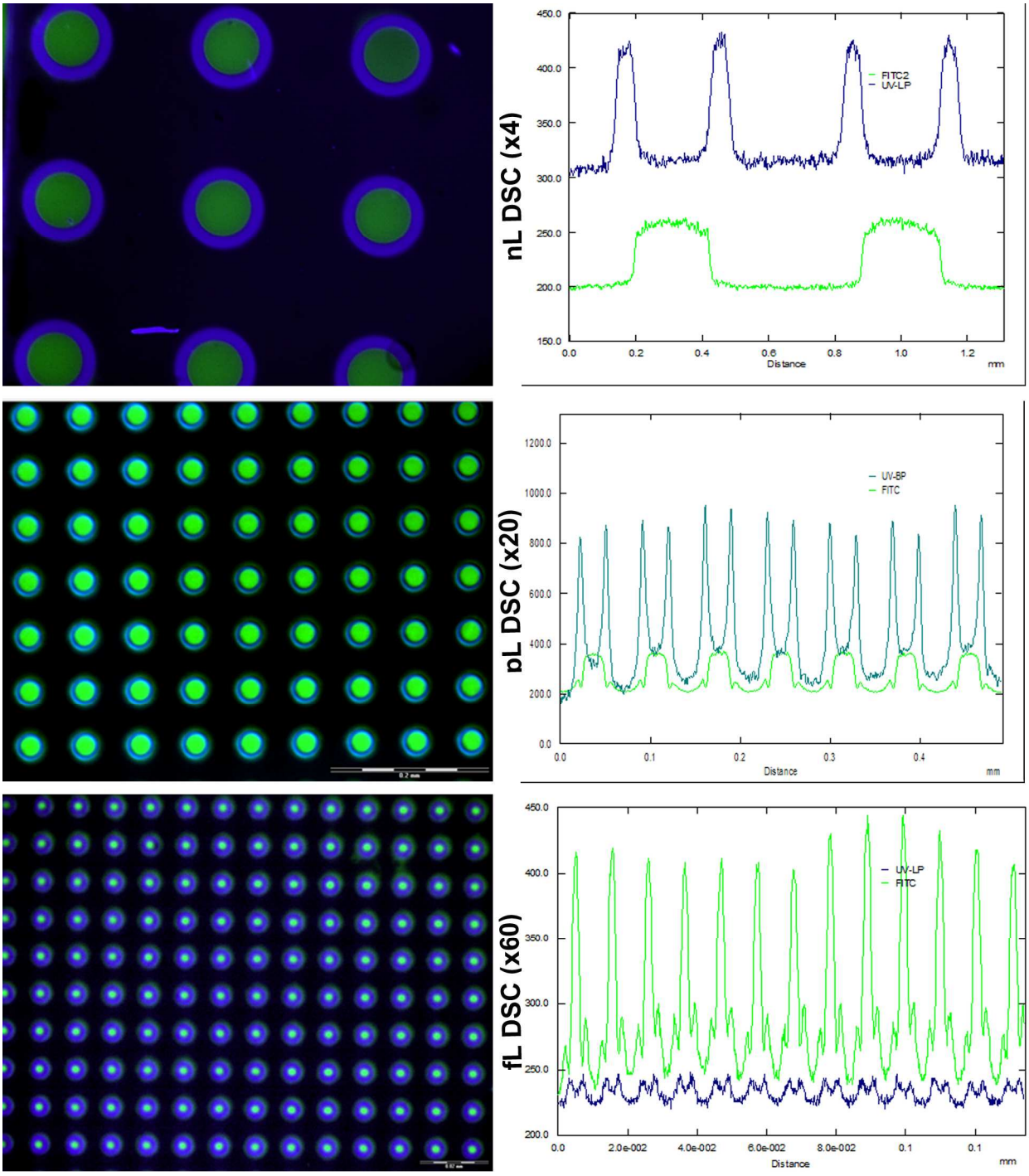
nL DSC (x4)
FITC2
UV-LP
Distance
mm
pL DSC (x20)
UV-BP
FITC
Distance
mm
fL DSC (x60)
UV-LP
FITC
Distance
mm

Figure 3

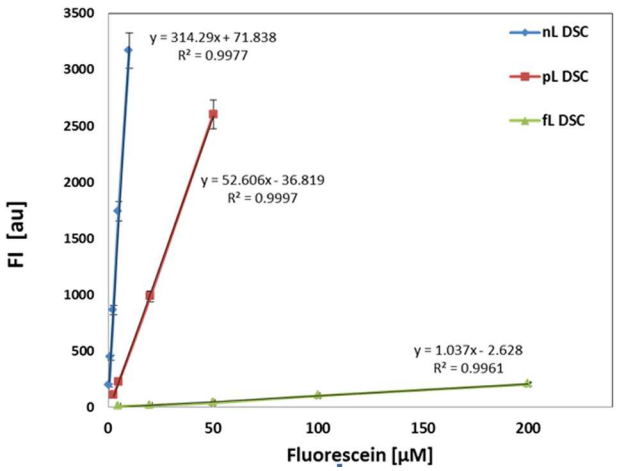
y = 314.29x + 71.838
R² = 0.9977
y = 52.606x - 36.819
R² = 0.9997
y = 1.037x - 2.628
R² = 0.9961
nL DSC
pL DSC
fL DSC
FI [au]
Fluorescein [µM]
0
500
1000
1500
2000
2500
3000
3500
0
50
100
150
200

Figure 4

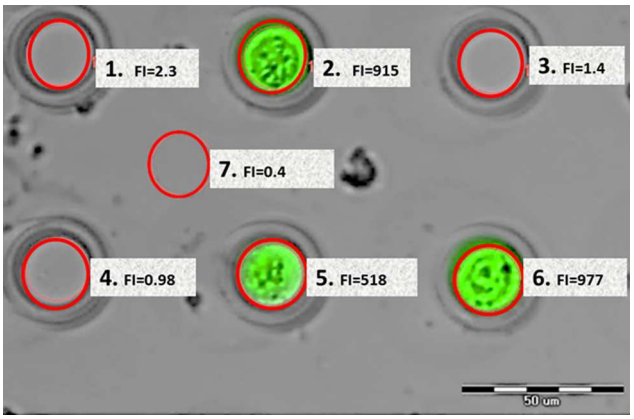

Figure 5

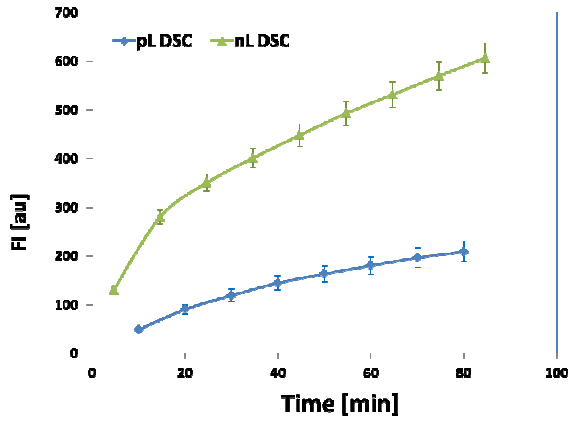
pL DSC
nL DSC
FI [au]
Time [min]
0
100
200
300
400
500
600
700
0
20
40
60
80
100

Figure 6

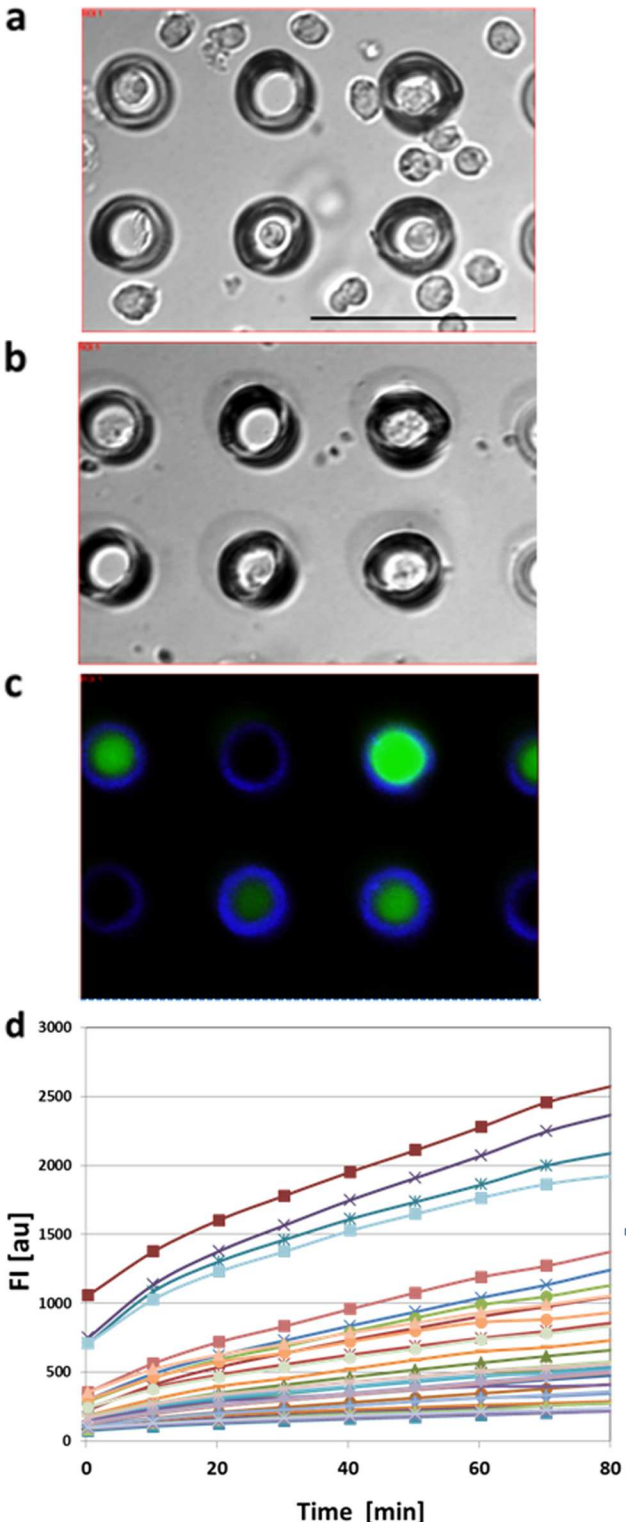

Figure 7

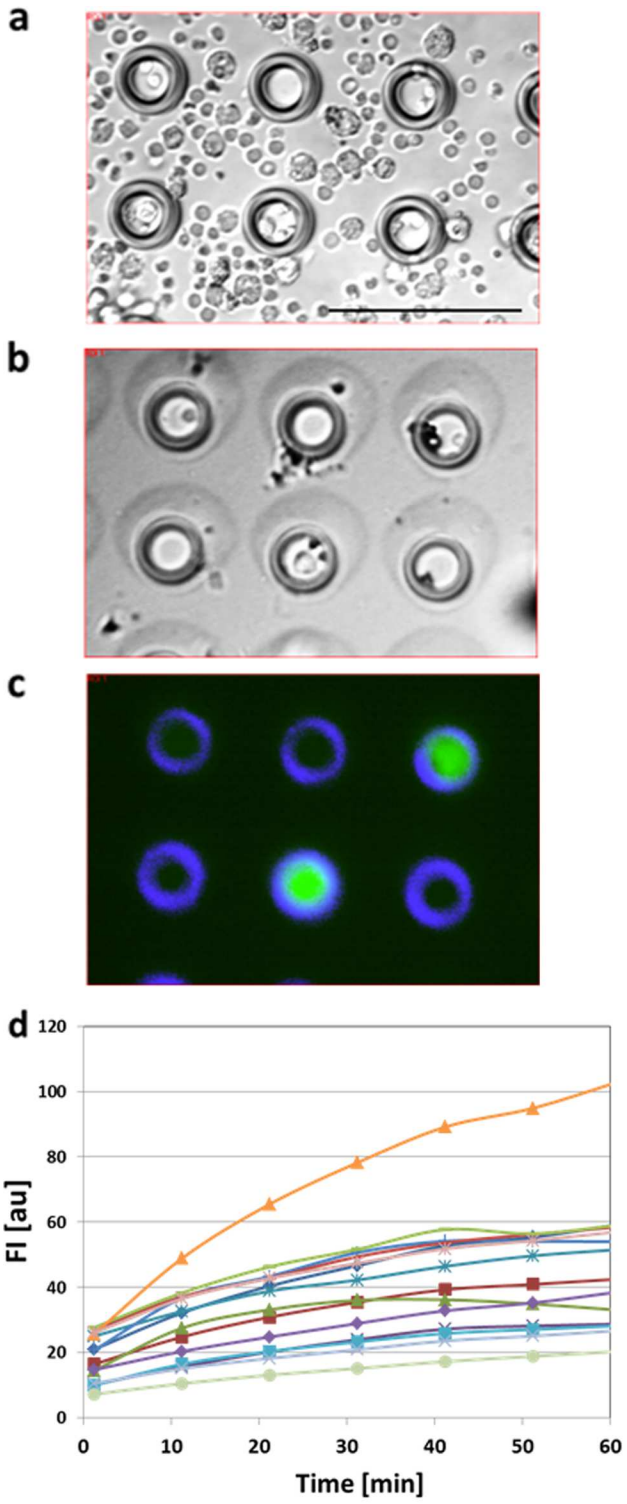

Figure 8

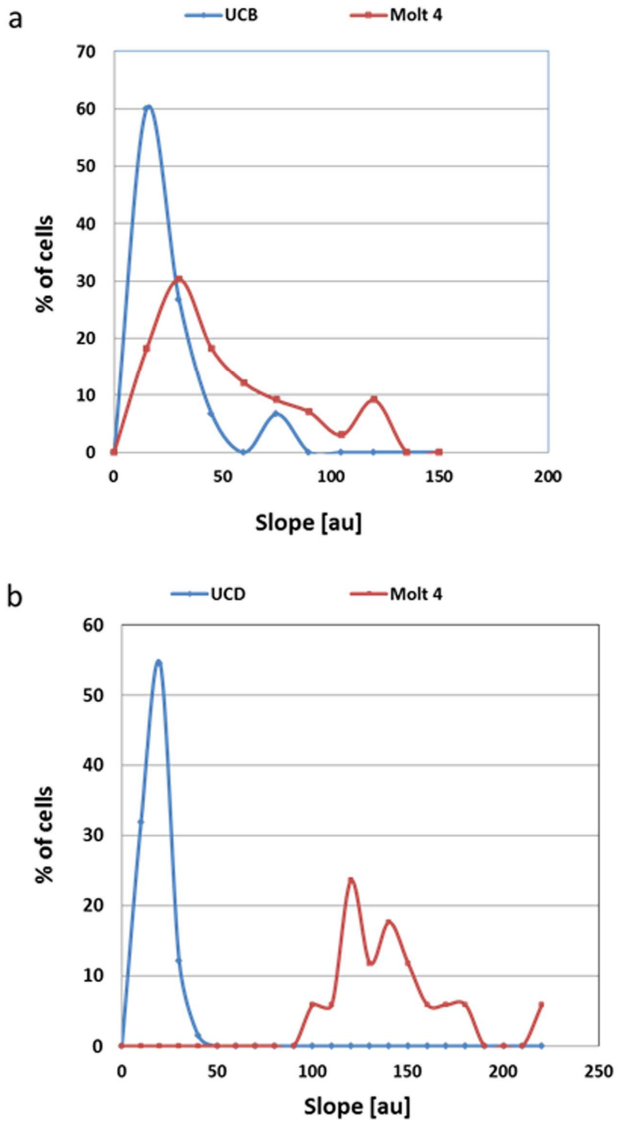

Figure 9

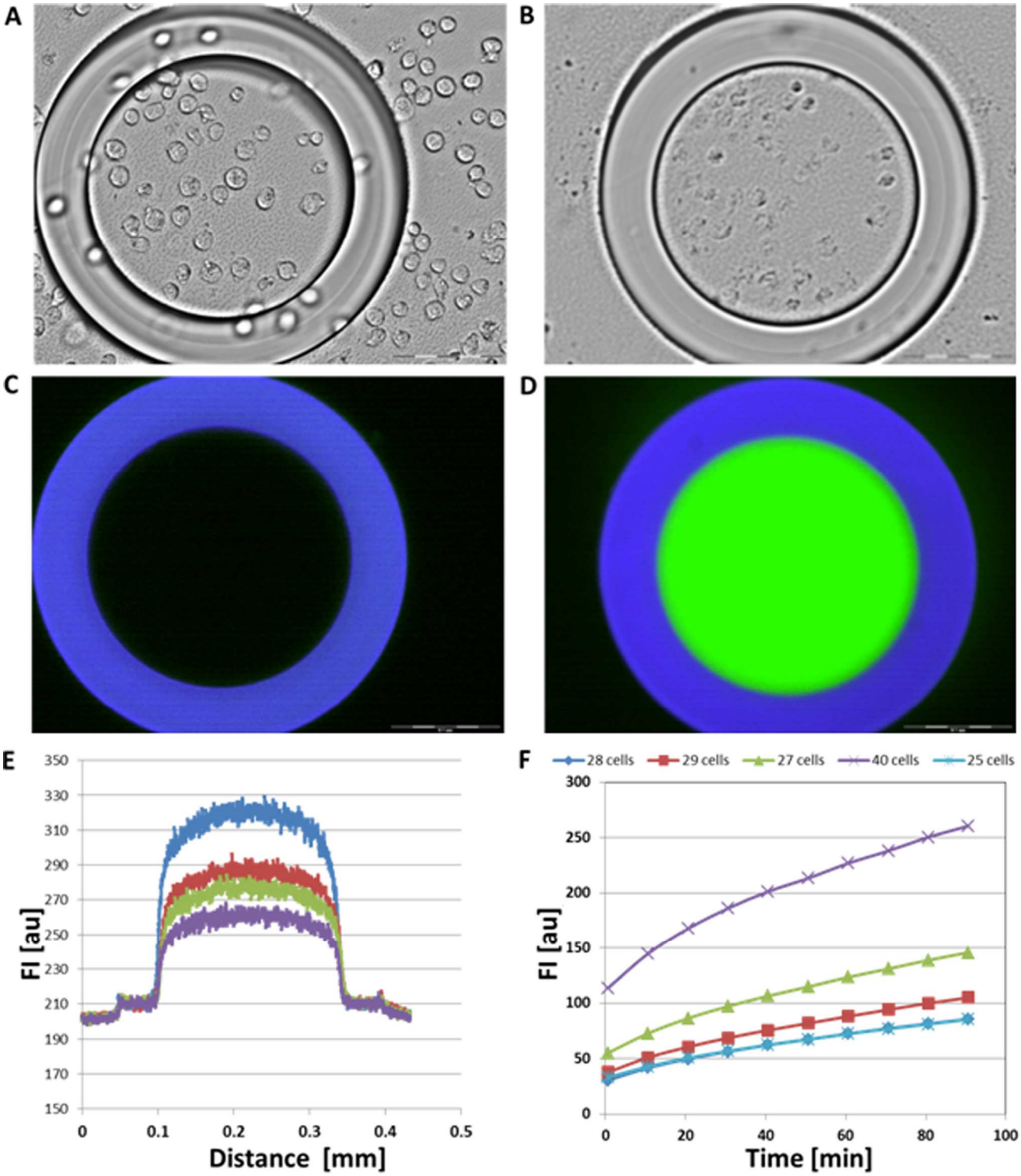
A
B
C
D
E
350
330
310
290
270
250
230
210
190
170
150
FI [au]
0
0.1
0.2
0.3
0.4
0.5
Distance [mm]
F
28 cells
29 cells
27 cells
40 cells
25 cells
300
250
200
150
100
50
0
FI [au]
0
20
40
60
80
100
Time [min]

Figure 10

Figure Captions

Figure 1

Schematic illustration of the DSC array sealing procedure. A solution droplet is poured on top of the pre-loaded DSC array, and covered with a layer of silicon sheet (A). Upon pressure, the solution between the individual DSCs is thrust aside, while the content of the chambers remains unaffected (B). OG stands for the optical glue NOA81 used in this study (see text for details).

Figure 2

Three types of DSCs arrays:

A – nL DSC array. Bright field images – left panel (x4, scale bar 500 μm); right panel (x10, scale bar 250 μm)

B – pL DSC array. SEM micrographs left panel (scale bar 500μm); SEM micrographs right panel (scale bar 50μm)

C – fL DSC array. Bright field image – left panel (x60 scale bar 20μm) and AFM image right panel (scale bar 20μm)

Figure 3

Overlapping images of UV (SU-8 auto fluorescence) and fluorescein fluorescence images (left panel) and the corresponding FI profiles of horizontal lines (right panel) of the nL (upper panels), pL (middle panels) and fL (lower panels) DSC arrays filled with fluorescein solutions. Note that chamber walls are indicated by the FI of the UV line, and the fluorescein solution is restricted to the inner volume of the chambers.

Figure 4

Changes in FI in response to increased concentrations of fluorescein solution loaded into the three types of DSCs. Each dot represents an average ± SD of four images taken at each fluorescein concentration.

Figure 5

Evaluation of chamber leakage and crosstalk. An overlaid image of bright field and fluorescence images of representative pL DSC array which was loaded with FDA stained Molt-4 T cells, followed by cell lysis, sealing and imaging after 100 min. The numbers represent seven ROIs; pL DSCs pre-occupied with colored cells (#2,5,6), empty chambers (#1,3,4) and the space in-between chambers (#7). The mean FI measured in all pixels within area of each ROI is indicated. Bar indicates 50μm.

Figure 6

Measurement of enzyme activity within pL and nL DSCs. Time dependent production of fluorescein by esterase from bulk cell lysate.

Figure 7

Monitoring FDA hydrolysis rates in Molt-4 individual cell lysate. Bright field image of pL DSC following loading of Molt-4 T cells (a), and after washing away of excess cells (b). An overlaid image of UV and fluorescein fluorescence images of the same pL DSCs following reaction initiation and chamber sealing (c). scale bar 100μm

Representative FI(t) curves of individual Molt-4 T cell lysate within pL DSCs, during esterase reaction measurement (d).

Figure 8

Monitoring FDA hydrolysis rates in UCB individual cell lysate. Bright field image of pL DSC following loading of UCB cells (a), and after washing away of excess cells (b). An overlaid image of UV and fluorescein fluorescence images of the same pL DSCs following reaction initiation and chamber sealing (c). scale bar 100μm

Representative FI(t) curves of individual UCB cell lysate within pL DSCs, during esterase reaction measurement (d).

Figure 9

Distribution histograms of enzyme activity in individual Molt-4 and UCB cell populations. Rate of FDA hydrolysis (slope) measured in individual cell lysate (A), and in intact live cells (B).

Figure 10

Esterase reaction in cell group lysate. Bright field (A,B) and fluorescence (C,D) images of a single nL DSC filled with a group of cells before (A,C) and after (B, D) cell lysis and initiation of enzymatic reaction. Changes in FI profile of a horizontal line in the nL DSC, during FDA hydrolysis reaction time (E). Rate of change in FI vs. time in Molt-4 T cell groups within individual nL DSCs (F).

Table 1

	fL DSC	pL DSC	nL DSC
Radius (µm)	1.28	12.8	120.5
Height (µm)	1.97	25.01	90.4
Volume	3.44 fL	12.87 pL	4.12 nL
Sensitivity (µM Fluorescein)	5	1	0.1
Sensitivity (# molecules)	1.06E+04	7.36E+06	2.95E+08

Volumes and sensitivity of the three types of DSCs. Volumes were calculated from chamber dimensions which were derived from SEM, AFM, bright field and auto-fluorescence images as described in Materials and Methods. Sensitivity was determined as the lowest fluorescein concentration that was statistically different from the blank. The minimum number of fluorescein molecules was calculated from the lowest fluorescein concentration in the corresponding DSC volume.

TOC Graphic

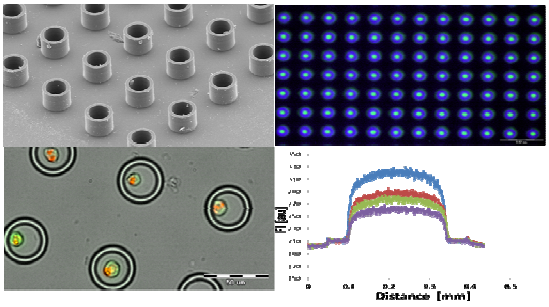

Micro-arrayed donut-shaped chambers (DSCs) in a range of volumes (fL to nL), have been developed and produced for various biochemical reaction measurements, and offer an inexpensive and simple system for live cell analysis and the corresponding single cell content.